Clinical PET of Neuroendocrine Tumors Using ^{64}Cu-DOTATATE: First-in-Humans Study

Andreas Pfeifer[1–3], Ulrich Knigge[2–4], Jann Mortensen[1,3], Peter Oturai[1,3], Anne Kiil Berthelsen[1,3], Annika Loft[1,3], Tina Binderup[1–3], Palle Rasmussen[5], Dennis Elema[5], Thomas Levin Klausen[1,3], Søren Holm[1,3], Eric von Benzon[1,3], Liselotte Højgaard[1,3], and Andreas Kjaer[1–3]

[1]Department of Clinical Physiology, Nuclear Medicine and PET, Rigshospitalet, Copenhagen, Denmark; [2]Cluster for Molecular Imaging, Faculty of Health Sciences, University of Copenhagen, Copenhagen, Denmark; [3]ENETS Center of Excellence for Neuroendocrine Tumors, Copenhagen, Denmark; [4]Department of Surgical Gastroenterology C, Rigshospitalet, Copenhagen, Denmark; and [5]Hevesy Laboratory, DTU-Risø, Roskilde, Denmark

The use of positron emitter–labeled compounds for somatostatin receptor imaging (SRI) has become attractive because of the prospect of improved spatial resolution, accelerated imaging procedures, and the ability to quantify tissue radioactivity concentrations. This paper provides results from first-in-humans use of ^{64}Cu-DOTATATE, an avidly binding somatostatin receptor ligand linked to a radioisotope with intermediate half-life and favorable positron energy (half-life, 12.7 h; maximum positron energy, 0.653 MeV). **Methods:** In a prospective setup, 14 patients with a history of neuroendocrine tumors underwent both PET/CT with ^{64}Cu-DOTATATE and SPECT/CT with our current routine imaging agent ^{111}In-diethylenetriaminepentaacetic acid–octreotide. After intravenous injection of 193–232 MBq of ^{64}Cu-DOTATATE, whole-body PET scans were acquired at 1 h (n = 14), 3 h (n = 12), and 24 h (n = 5) after administration. Tissue radioactivity concentrations for normal organs and lesions were quantified, and standardized uptake values were calculated for the early (1 h) and delayed (3 h) scans. Using the data for 5 patients, we assessed the radiation dose with OLINDA/EXM software. Furthermore, the clinical performance of ^{64}Cu-DOTATATE with respect to lesion detection was compared with conventional SRI. **Results:** SRI with ^{64}Cu-DOTATATE produced images of excellent quality and high spatial resolution. Images were characterized by high and stable tumor-to-background ratios over an imaging time window of at least 3 h. Compared with conventional scintigraphy, ^{64}Cu-DOTATATE PET identified additional lesions in 6 of 14 patients (43%). In 5 patients, lesions were localized in organs and organ systems not previously known as metastatic sites, including the early-stage detection of a secondary neuroendocrine tumor in a patient with a known mutation in the multiple endocrine neoplasia type I gene. All major additional findings seen only on PET could be confirmed on the basis of a clinical follow-up interval of 18 mo. Calculated radiation dose estimates yielded an effective dose of 6.3 mSv for an injected activity of 200 MBq of ^{64}Cu-DOTATATE, with the liver being the organ with the highest absorbed radiation dose (0.16 mGy/MBq). **Conclusion:** This first-in-humans study supports the clinical use of ^{64}Cu-DOTATATE for SRI with excellent imaging quality, reduced radiation burden, and increased lesion detection rate when compared with ^{111}In-diethylenetriaminepentaacetic acid–octreotide.

Key Words: neuroendocrine tumors; ^{64}Cu-DOTA-Tyr^3-octreotate; positron-emission tomography; ^{111}In-DTPA-octreotide; first-in-humans study

J Nucl Med 2012; 53:1207–1215
DOI: 10.2967/jnumed.111.101469

Somatostatin receptor imaging (SRI) is specific and the most sensitive imaging modality in the evaluation of well-differentiated neuroendocrine tumors (NETs) (*1–3*). SRI embraces a typical feature of this tumor entity, namely NET overexpression of cell surface–bound somatostatin receptors (*4*). These receptors can be directly targeted by radiolabeled somatostatin analogs (*5,6*). Given a sufficient signal-to-noise ratio, accumulation of the radiotracer is typically detected by a combination of planar whole-body scintigraphy and SPECT or, more recently, PET. The challenge of precise anatomic mapping has been overcome by the adoption of dual-modality imaging systems (SPECT/CT, PET/CT). Currently, SRI with the SPECT agent ^{111}In-diethylenetriaminepentaacetic acid (DTPA)–octreotide (Octreoscan; Covidien) has yet to be considered the standard method, as is reflected by the current guidelines of international scientific organizations with special interest in this field (*7,8*). However, PET is superior to SPECT in both sensitivity and spatial resolution. Furthermore, PET enables quantitation of tissue radioactivity concentrations. As a consequence, several ^{68}Ga-labeled somatostatin analogs have attracted the attention of the nuclear medicine community (*9*). Compared with conventional SRI, increased detection rates have been reported using ^{68}Ga-labeled somatostatin analogs (*2,10*). Besides limiting factors arising from geometric features of the scanner systems (e.g., detector crystal size), the spatial resolution of PET is confined by the positron energy of the used isotope (*11,12*). From that

Received Dec. 5, 2011; revision accepted Mar. 13, 2012.
For correspondence or reprints contact: Andreas Kjaer, Department of Clinical Physiology, Nuclear Medicine and PET, KF-4012 Rigshospitalet, Blegdamsvej 9, DK-2100 Copenhagen, Denmark.
E-mail: akjaer@sund.ku.dk
Published online Jul. 10, 2012.

perspective, it seemed promising to label DOTATATE with ^{64}Cu (17% β^+; maximum positron energy, 0.653 MeV; half-life [$t_{1/2}$], 12.7 h), an intermediate-half-life, low-energy positron emitter with a positron range comparable to that of ^{18}F (97% β^+; maximum positron energy, 0.633 MeV; $t_{1/2}$, 109.7 min) but considerably lower than that of ^{68}Ga (88% β^+; maximum positron energy, 1.899 MeV; $t_{1/2}$, 68 min). Unlabeled DOTATATE has previously been shown to have particularly high affinity for human somatostatin receptor 2, the subtype primarily overexpressed in NETs (*13–15*). Accordingly, our rationale for the choice of ^{64}Cu-DOTATATE was to use a high-affinity somatostatin receptor ligand labeled with a short-range positron emitter with an intermediate half-life to extend the imaging time window during the ongoing clearing of background activity, expectedly leading to a better tumor-to-background ratio (TBR). Furthermore, because ^{177}Lu-DOTATATE seems to be the ligand of choice for therapy of NETs at many institutions, ^{64}Cu-DOTATATE imaging may be used for dose calculation in those patients to tailor radionuclide therapy.

The aim of this first-in-humans study was, therefore, to validate the clinical use of ^{64}Cu-DOTATATE, including biodistribution and image quality, and to establish the optimal image acquisition times. In addition, we obtained radiation dose estimates and explored the clinical performance of ^{64}Cu-DOTATATE PET regarding lesion detection ability in comparison with ^{111}In-DTPA-octreotide SPECT.

MATERIALS AND METHODS

Synthesis of ^{64}Cu-DOTATATE

^{64}Cu was produced via the ^{64}Ni(p,n)^{64}Cu reaction using a solid target system comprising a water-cooled target mounted on the beam line of a PETtrace (GE Healthcare) cyclotron (*16*). The target consisted of ^{64}Ni metal (enriched to >99%) electroplated on a silver disk backing. For this specific type of production, a proton beam with an energy of 16 MeV and a beam current of 20 μA was used. After irradiation, the target was transferred to the laboratory for further chemical processing in which the ^{64}Cu was isolated using ion exchange chromatography. Final evaporation from aqueous HCl yielded 2–6 GBq of ^{64}Cu as $^{64}CuCl_2$ (specific activity, 300–3000 TBq/mmol; radionuclidic purity, >99%). DOTATATE was labeled with ^{64}Cu by adding a sterile solution of DOTATATE (0.3 mg) and gentisic acid (25 mg) in aqueous sodium acetate (1 mL; 0.4 M, pH 5.0) to a dry vial containing $^{64}CuCl_2$ (800–1,000 MBq). Gentisic acid was added as a scavenger to reduce the effect of radiolysis. The mixture was left at ambient temperature for 10 min and then diluted with sterile water (1 mL). Finally, the mixture was passed through a Millex-GP 0.22-μm sterile filter (Millipore). Radiochemical purity was determined by reversed-phase high-pressure liquid chromatography (RP-HPLC), and the amount of unlabeled $^{64}Cu^{2+}$ was determined by thin-layer chromatography (TLC). All chemicals were purchased from Sigma-Aldrich Denmark A/S unless specified otherwise. DOTATATE was purchased from Bachem. ^{64}Ni was purchased at more than 99% purity from Campro Scientific GmbH. All solutions were made using ultrapure water (<0.07 μS/cm). RP-HPLC was performed on an Alliance 2795 Separations module equipped with a 2489 ultraviolet/visible detector (Waters Corp.) and a 105 S-1 radioactivity detector (Caroll-Ramsey Associates) (RP-HPLC column, Luna C18, HST, 50 × 2 mm, 2.5 μm [Phenomenex]). The mobile phase was 5% aqueous acetonitrile (0.1% trifluoroacetic acid) and 95% aqueous acetonitrile (0.1% trifluoroacetic acid). TLC was performed using a Raytest MiniGita Star scanner equipped with a β-detector. The eluent was 50% aqueous methanol, and the TLC plate was a Silica60 on aluminum foil (Sigma-Aldrich Denmark A/S). Ion exchange chromatography was accomplished on a Dowex 1 × 8 resin (Lenntech) chloride form (200–400 mesh).

Patient and Inclusion Criteria

Fourteen patients with histopathologically confirmed NETs were enrolled in the study from November 2009 to January 2010. Patients were offered study inclusion if they were referred for conventional SRI as part of their routine follow-up. PET and SPECT scans were obtained within 60 d in random order. Local clinical routine does not require withdrawal of long- or short-acting somatostatin analogs. The study group consisted of 13 patients with gastroenteropancreatic NETs and 1 patient with a known mutation in the multiple endocrine neoplasia type I gene, who was diagnosed with a bronchogenic NET 10 y earlier. Ages ranged from 40 to 80 y, and there were 4 women and 10 men. Twelve patients were in advanced disease stages (TNM stage IV according to the most recent classifications of the American Joint Committee on Cancer/International Union Against Cancer and the European Neuroendocrine Tumor Society) (*17–19*). Two patients had undergone resection, one without and the other with microscopic residual tumor, and neither had detectable disease at the time the manuscript for this article was prepared. Detailed patient characteristics are given in Table 1. Patients 1–4 and 6 were used for the dosimetry calculations. The tumor burden varied between the patients, and 2 patients had no tumor uptake, making dosimetry representative for all NET patients. All patients had given written informed consent before inclusion. The study was approved by the Regional Scientific Ethical Committee (protocol H-D-2008-045).

Image Acquisition and Reconstruction

PET/CT. Data acquisition was performed using a Biograph 64 TruePoint PET/CT scanner (Siemens Medical Solutions) with an axial field of view of 216 mm and a transaxial field of view of 205 mm. Axial and transaxial resolutions were 4.7 and 4.2 mm, respectively. After intravenous injection of 193–232 (mean, 207) MBq of ^{64}Cu-DOTATATE, emission scans were acquired 1 h (n = 14), 3 h (n = 12), and 24 h (n = 5) after administration. Whole-body PET scans (skull to mid thigh) were obtained in 3-dimensional mode, with an acquisition time of 3 min per bed position. CT data were used for attenuation correction. PET data were reconstructed with the TrueX (Siemens Medical Solutions) algorithm using 3 iterations and 21 subsets and smoothed by a gaussian filter (full width at half maximum, 2 mm). A diagnostic CT scan was obtained before the first PET scan, with a 3-mm slice thickness, 120 kV, and a quality reference of 225 mAs modulated by the Care Dose 4D automatic exposure control system (Siemens Medical Solutions). A low-dose CT scan was acquired before each of the subsequent scans and used for attenuation correction. An automatic injection system was used to administer 75 mL of an iodine-

TABLE 1
Patient Characteristics

Patient no.	Primary	Sex	Age at study inclusion (y)	Time since diagnosis (mo)	Primary resected?	Ki67 percentage	Syndrome	TNM*	Metastases	^{18}F-FDG
1	Cecum	M	58	195	Yes	Not performed	Carcinoid	IV	Carcinomatosis	Positive
2	Duodenum	F	50	97	Yes	1	Gastrinoma	R0		Negative
3	CUP	M	44	16	No	5	Carcinoid	IV	Peritoneum	Not performed
4	Ileum	M	62	9	Yes	3	None	R1		Not performed
5	Ileum	M	63	88	Yes	3	Carcinoid	IV	Lymph nodes	Negative
6	CUP	F	40	23	No	5	Carcinoid	IV	Liver	Negative
7	Pancreas	M	72	2	No	7	None	IV	Liver, bones	Not performed
8	Lower small intestine	F	51	92	Yes	3	Carcinoid	IV	Liver, breasts	Negative
9	CUP	M	81	3	No	10	Carcinoid	IV	Liver, peritoneum	Positive
10	Ileum	M	64	10	Yes	1	None	IV	Lymph nodes	Not performed
11	CUP	M	64	38	No	4	Carcinoid	IV	Liver	Positive
12	Ileum	M	72	6	No	10	Carcinoid	IV	Liver, bones, lymph nodes	Not performed
13	Bronchogenic NET	F	44	103	No	5	Carcinoid	IV	Lungs, lymph nodes	Positive
14	CUP	M	76	3	No	7	Carcinoid	IV	Liver	Positive

*TNM stage before study inclusion according to most recent classifications of European Neuroendocrine Tumor Society and American Joint Committee on Cancer/International Union Against Cancer.

R0 resection = complete resection, no microscopic residual tumor; CUP = cancer of unknown primary; R1 resection = microscopic residual tumor.

containing contrast agent (Optiray 300; Covidien) with a scan delay of 60 s and flow rate of 1.5 mL/s, followed by an injection of 100 mL of NaCl with a flow rate of 2.5 mL/s. Furthermore, patients had been asked to drink 500 mL of water 25 min before image acquisition.

SPECT/CT. Dual-head hybrid SPECT/CT cameras were used for planar and tomographic imaging (Precedence 16-slice scanner [Philips Healthcare] and VG Hawkeye [GE Healthcare]). An activity of 197–227 (mean, 207) MBq of ^{111}In-DTPA-octreotide was administered intravenously. Planar images were acquired at 24 h (anterior and posterior whole-body; scan speed, 5 cm/min; matrix, 512 × 1,024) and 48 h after injection (15-min static planar image [256 × 256 matrix] of the abdomen using a large-field-of-view medium-energy collimator). SPECT (20 s/step, 128 angles, 128 × 128 matrix) over the abdomen (and chest if pathologic lesions were suspected from planar scintigraphy) was obtained at 24 or 48 h. A low-dose CT scan (20 mA, 140 kV [Precedence] or 2.5 mA, 140 kV [Hawkeye]) was used as an anatomic guide and for attenuation correction. Attenuation- and scatter-corrected SPECT and CT scans were fused and reviewed on dedicated workstations (EBW [Philips Healthcare] and eNTEGRA [GE Healthcare]) after reconstruction using standard iterative algorithms.

Visual Image Analysis and Activity Quantification

PET/CT and SPECT/CT images were analyzed separately by 2 different teams consisting of 2 experienced readers. The 2 teams were masked to the images and readings of the other team. Lesions discovered on the fused PET/CT or SPECT/CT images had to be a clearly detectable on the somatostatin receptor images to be categorized as an SRI-positive finding. To establish a reference method, CT data were masked for both SPECT and PET and additionally evaluated by an experienced radiologist. The absolute number of lesions per organ system was obtained with a numeric limitation of 10 lesions per organ and 30 positive findings for lymph nodes per patient. ^{64}Cu-DOTATATE PET scans were obtained with a single coregistered contrast-enhanced high-dose CT scan per patient. Half of the ^{111}In-DTPA-octreotide SPECT scans were obtained using diagnostic CT, whereas the other half were obtained using low-dose CT for reasons of radioprotection. Because of the lack of biopsy specimen, suspected lesions were confirmed by supplementary cross-sectional imaging (CT, ultrasonography) and conventional SRI during a follow-up of 18 mo. PET images in units of Bq/mL were used for quantitative analysis of tissue radioactivity concentrations for dosimetry purposes and for calculation of maximal standardized uptake values (SUVmax). The latter uptake characteristic was obtained by drawing spheric volumes of interest (VOIs) sufficiently large to encompass the whole lesion—that is, including a rim of surrounding normal tissue. SUVmax was calculated from the generated VOI for the early (1 h) and delayed (3 h) scans and reported only for those lesions with the highest tracer uptake per organ or organ system (standardized uptake value [SUV] = decay-corrected tissue concentration/[injected activity/body weight]). For the calculation of absorbed dose estimates, we assumed a uniform distribution of radioactiv-

ity concentrations throughout the source organs. In a manner similar to SUV calculation, 3 sufficiently large spheric VOIs were drawn in representative areas of each source organ by carefully avoiding the inclusion of metastatic lesions. The obtained mean activity concentrations were averaged, and total organ activity concentrations were calculated by multiplying these values by organ masses of the OLINDA male adult phantom (*20*). As a surrogate for red marrow activity, VOIs were drawn encompassing large portions of the L3–L5 vertebrae. Because bowel wall activity could not be distinguished from bowel content activity, freehand regions of interest were drawn over areas of maximum activity on 3 adjacent slices. Up to 24 h, the cumulated activities were estimated by adding the areas under a curve defined by the measured, decay-uncorrected time–activity data of the 3 imaging time points. The curve was constructed as a linear piece from injection to the first measuring point and monoexponentials between the measuring points. Beyond 24 h (last imaging point), removal by simple physical decay was assumed. Organ-normalized cumulated activity was obtained by dividing the cumulated activity of each source organ by the injected activity. Values of all 5 patients were averaged. Because no urine samples were collected, a minimum urinary excretion fraction was estimated from the 3 h PET scans by taking activity concentrations from VOIs drawn inside the urinary bladder and multiplying by the bladder volume calculated from coregistered CT data. Consistent with the assumption of pure physical decay after the 3 h data point, no further excretion was assumed. Cumulated activity in muscle was calculated from measured VOIs in the manner done for other organs. The value assigned to the remainder of the body was derived as the residual between the total cumulated activity (as calculated from the nuclide's half-life) minus all activity accounted for in specific organs (including muscle) or by excretion.

All data were entered into OLINDA/EXM software to obtain corresponding estimates of organ-absorbed doses and effective dose.

An estimate of the absorbed dose to the pituitary gland was calculated using the unit density sphere model in OLINDA/EXM (*20*) and, again, assuming only physical decay after 24 h.

RESULTS

Radiochemistry and Toxicity

The labeling of ^{64}Cu-DOTATATE took less than 30 min and resulted in greater than 95% yield, as shown with radio-RP-HPLC. No additional radiochemical purification step was required. The amount of unlabeled ^{64}Cu in the product was less than 1%, as demonstrated by radio-TLC. The specific activity of ^{64}Cu-DOTATATE was 4.78 MBq/mmol. The mean ± SD of the administered mass of ^{64}Cu-DOTATATE was 33.9 ± 1.7 ng (range, 31.7–38.0 ng). The mean administered activity was 207 ± 10 MBq (range, 193–232 MBq). There were no adverse or clinically detectable pharmacologic effects in any of the 14 subjects, except for 4 who experienced self-limiting nausea of seconds to a few minutes duration immediately after injection. This side effect was probably due to the somatostatin analog contained in the tracer. No significant changes in vital signs were observed.

Biodistribution of ^{64}Cu-DOTATATE

A characteristic imaging series illustrating activity biodistribution at 1, 3, and 24 h after injection is shown in Figure 1.

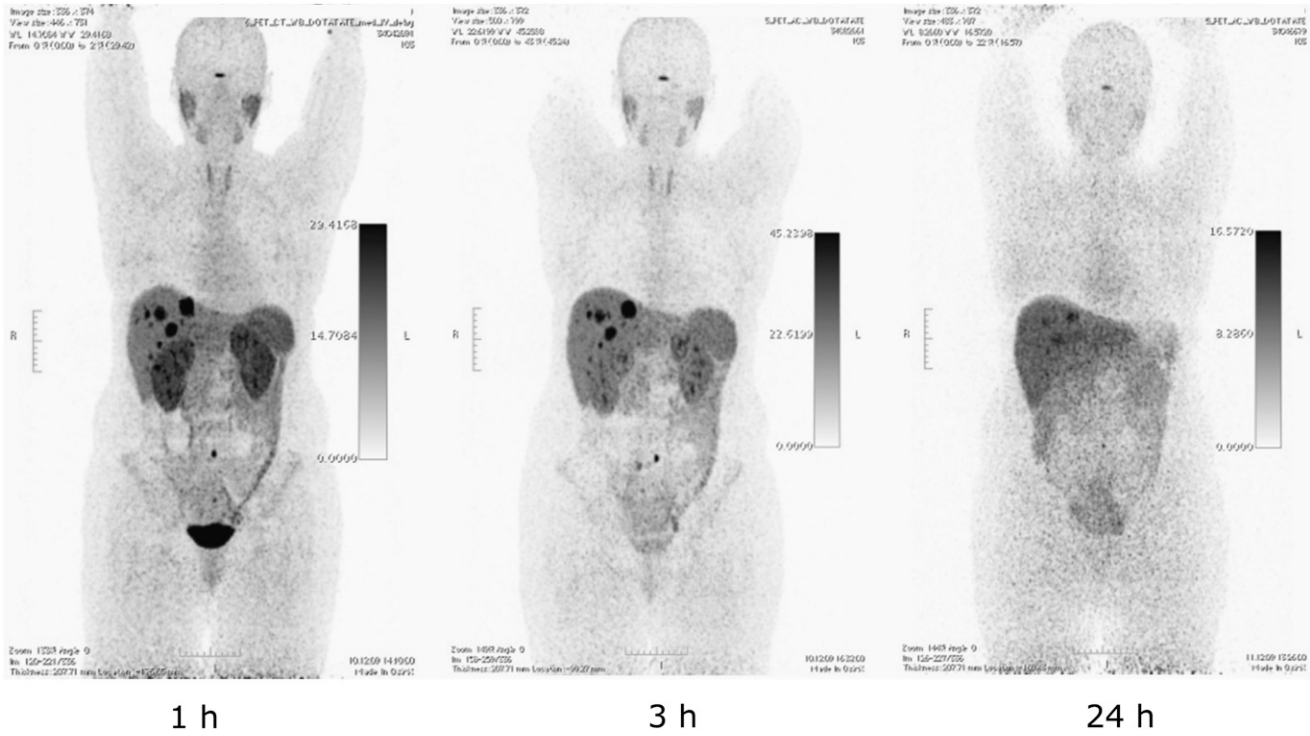

FIGURE 1. ^{64}Cu-DOTATATE PET (maximum-intensity projections) at 1, 3, and 24 h in same patient with gastroenteropancreatic NET with liver metastases.

On the basis of SUV quantitation, tracer accumulation was classified in the following 3 categories: high, moderate, and faint. High accumulation of ^{64}Cu-DOTATATE was seen in the pituitary (averaged SUVmax ± SEM at 1 h and 3 h, 19.0 ± 2.6 and 19.4 ± 3.3, respectively), adrenal glands (21.1 ± 3.1 and 27.8 ± 3.6, respectively), kidneys (21.3 ± 2.5 and 19.9 ± 2.0, respectively), renal pelvis, and urinary bladder. Moderate to high uptake was observed in the liver (11.3 ± 0.8 and 13.6 ± 0.8, respectively) and spleen (17.8 ± 1.8 and 18.0 ± 1.8, respectively). The salivary glands showed faint to moderate uptake in 12 of 14 patients. In 2 patients, moderate tracer accumulation was observed in the thyroid gland, with a diffuse distribution pattern in one patient and a focal pattern in the other. In most patients, numerous lesions were clearly delineated from surrounding tissue (background), showing tracer uptake ranging from moderate to intense (SUVmax range at 1 h and 3 h: liver lesions, 20–81 and 26–81, respectively; bone lesions, 30–117 and 27–111, respectively; and lymph nodes, 9–110 and 9–115, respectively). The TBRs were correspondingly high (1 h and 3 h: liver lesions, 2:1 and 7:1, respectively; bone lesions, 4:1 and 8:1, respectively; and lymph nodes, 3:1 and 19:1, respectively). Background reference SUVmax for lymph nodes was calculated from VOIs drawn over the lumbar part of the psoas muscle, and reference SUVmax for bones was generated by drawing VOIs over contralateral or adjacent normal bone. SUVmax of the early and delayed images remained relatively stable (variability ≤ 20%) for tissues that had known high physiologic somatostatin receptor density and did not take part in tracer or activity excretion (i.e., pituitary, adrenals, and spleen). The same was true for most lesions. Conversely, higher time-dependent intrapatient variability for SUVmax was observed for the kidneys, corresponding with urinary tracer excretion as demonstrated by activity accumulation in the renal pelvis and urinary bladder seen only on the early and delayed images. As a possible sign of hepatobiliary excretion, an increase in SUVmax from the 1 h to the 3 h scan in normal liver tissue ranged from 10% to 65% among patients. This finding was in line with visible activity localized to the gallbladder on 3 h images, which was not apparent on images from the early acquisition. Images of the late scan (24 h) were characterized by activity washout from most organs and lesions, whereas activity retention in the liver and activity accumulation in the intestines became apparent. No activity was visible in the renal collecting system or urinary bladder at the late time point.

Table 2 depicts normalized cumulated activity for source organs. Table 3 shows the associated absorbed dose estimates based on an estimated urinary excretion fraction of 10%, with a presumed 2-h voiding interval and a biologic half-life of 1 h. The dose calculations yielded an effective dose of 0.0315 mSv/MBq. Apart from the pituitary gland, which was estimated to receive an absorbed dose of 0.19 mGy/MBq, the liver was the organ with the highest absorbed dose (0.16 mGy/MBq), followed by the kidneys (0.14 mGy/MBq).

TABLE 2
Organ Normalized Cumulated Activity

Source organ	Mean (MBq h/MBq)	SE (MBq h/MBq)
Adrenals	2.65E−02	1.19E−02
Gallbladder	1.50E−02	6.71E−03
Lower large intestine contents	9.74E−02	4.36E−02
Small intestine contents	5.23E−01	2.34E−01
Kidneys	4.78E−01	2.14E−01
Liver	3.33E+00	1.49E+00
Muscle	4.23E+00	1.89E+00
Pancreas	9.40E−02	4,20E−02
Red Marrow	3.59E−01	1.60E−01
Spleen	2.40E−01	1.07E−01
Urinary bladder contents	1.10E−01	—
Remainder	7.23E+00	3.23E+00

Comparative Lesion Detection

In an organ-based comparison of the 2 SRI modalities, ^{64}Cu-DOTATATE PET detected additional lesions in 6 of 14 patients (43%). All lesions detected on ^{111}In-DTPA-octreotide SPECT were also detected on ^{64}Cu-DOTATATE PET. In 5 patients, the additional lesions were localized in

TABLE 3
Absorbed Doses

Target organ	Mean* absorbed dose (mGy/MBq)
Adrenals	1.37E−01
Brain	1.27E−02
Breasts	1.32E−02
Gallbladder wall	3.96E−02
Lower large intestine wall	4.32E−02
Small intestine	6.55E−02
Stomach wall	1.93E−02
Upper large intestine wall	2.18E−02
Heart wall	1.86E−02
Kidneys	1.39E−01
Liver	1.61E−01
Lungs	1.67E−02
Muscle	1.90E−02
Ovaries	1.92E−02
Pancreas	9.27E−02
Red marrow	2.65E−02
Osteogenic cells	3.35E−02
Skin	1.22E−02
Spleen	1.15E−01
Testes	1.36E−02
Thymus	1.49E−02
Thyroid	1.41E−02
Urinary bladder wall	3.70E−02
Uterus	1.89E−02
Total body	2.50E−02

*Mean of 5 patients.
Effective dose (mSv/MBq) was 3.15E−02.

organs or organ systems not previously recognized as metastatic sites: lung lesions (patient 1), a single-bone metastasis and hepatic lesions (liver lesions were known from previously performed CT; patient 8), bone metastases and lymph nodes (patient 9), peritoneal carcinomatosis (patient 12), pancreatic and pulmonary lesions (pulmonary lesions were known; patient 13), and a brain metastasis and a single-bone lesion (patient 14). All foci detected by ^{64}Cu-DOTATATE PET but not by ^{111}In-DTPA-octreotide SPECT were retrospectively assessed as being true-positive lesions, with the exception of the bone lesions in patients 9 and 14. Thus, in these 6 patients, one or more of the additional lesions found by PET were confirmed. ^{64}Cu-DOTATATE PET revealed in general more lesions ($n > 219$, including 98 lymph nodes) than conventional SRI ($n > 105$, including 29 lymph nodes). A common feature of nearly all additionally discovered lesions was their diminutive size (Fig. 2).

Table 4 gives a more detailed overview of the results from the findings of the 2 SRI modalities, coregistered diagnostic CT, and follow-up imaging. Figure 3 shows the pancreatic lesions of the patient known with multiple endocrine neoplasia type I syndrome (patient 13) on a ^{64}Cu-DOTATATE PET/CT slice and on an equivalent contrast-enhanced late arterial-phase CT slice obtained 6 mo later. Figure 4 illustrates the cerebral lesion of patient 14 seen on ^{64}Cu-DOTATATE PET but not on ^{111}In-DTPA-octreotide SPECT.

DISCUSSION

In this first-in-humans study, we found that PET with ^{64}Cu-DOTATATE provided considerably better image quality than SPECT with ^{111}In-DTPA-octreotide, resulting in a higher lesion detection rate for ^{64}Cu-DOTATATE PET than for ^{111}In-DTPA-octreotide SPECT. In 5 patients (36%), ^{64}Cu-DOTATATE PET revealed lesions in organs not previously known as metastatic sites. This finding is of special interest because it may lead to more accurate staging, which in turn may critically affect the therapeutic management of NET patients. In no case did ^{111}In-DTPA-octreotide SPECT detect lesions that were not also detected by ^{64}Cu-DOTATATE PET. Organ-specific absorbed dose estimates are given in Table 3. On the basis of the dosimetry data for the 5 patients, ^{64}Cu-DOTATATE PET was associated with a lower radiation dose than after a standard administered activity of ^{111}In-DTPA-octreotide. Despite known shortcomings and the limited number of patients, this result can be considered rather robust. Applying tissue-weighting factors according to IRCP 60 (*21*), and given the 200-MBq injected activity, we can determine that ^{64}Cu-DOTATATE delivered an estimated effective dose of 6.3 mSv to the patients, compared with 12 mSv for ^{111}In-DTPA-octreotide for a standard administered activity (*8*). Conventional SRI with ^{111}In-DTPA-octreotide usually follows a 2 d protocol. In contrast, the time required for SRI is considerably reduced when using ^{64}Cu-DOTATATE because of the accelerated imaging procedures offered by the physical and pharmacokinetic features of this tracer. As shown by our study, image acquisition can be initiated at 1 h after administration of ^{64}Cu-DOTATATE. High spatial resolution was illustrated by sharp images, allowing for distinct delineation of small organs with appreciable somatostatin receptor expression such as the adrenals and the pituitary. High image contrast could be demonstrated by notably high TBRs, even in organs with physiologic high somatostatin receptor density such as the pancreas. In accordance with this is the detection of an additional pancreatic lesion (TBR, 6:1) in patient 13 with known multiple endocrine neoplasia type I syndrome. Despite enhanced clinical awareness and a consecutive diagnostic exploration by endoscopic ultrasonography, validation of the lesion shown on PET was not achieved until 6 mo later by contrast-enhanced CT, demonstrating a lesion size of 6 mm.

Obvious advantages of PET systems, such as enhanced photon sensitivity and reduced acquisition times, have paved the way for the clinical implementation of positron emitter–linked somatostatin analogs. Furthermore, the spatial resolution achievable by PET is generally higher than that by SPECT. However, a limiting factor for high-resolution PET is the positron energy of the used isotope (*22*). The use of isotopes with a lower positron energy is therefore considered advantageous and may result in reduced image blurring because of correspondingly shorter positron ranges. That impact is considered to be modest in human state-of-the art whole-body PET scanners with intrinsic spatial resolution on the order of 4–6 mm in full width at half maximum (*11*). However, the impact of positron energy may become more decisive as PET scanner technology continues to advance (*23,24*). Not surprisingly, given the physical properties discussed here, the current head-to-head

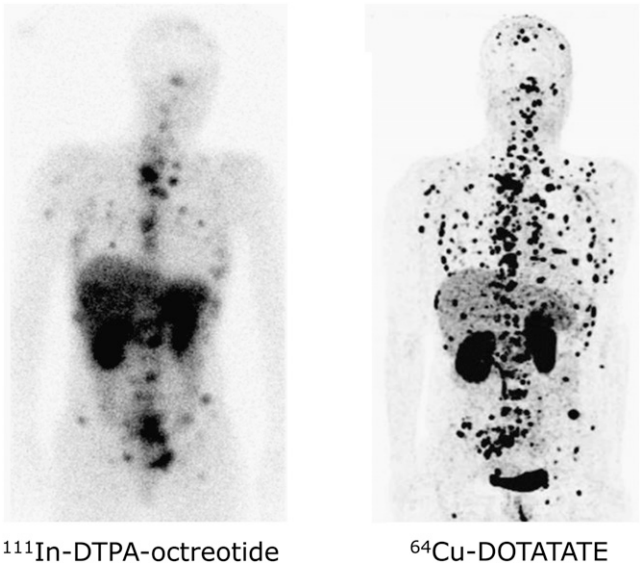

FIGURE 2. Comparison of ^{111}In-DTPA-octreotide and ^{64}Cu-DOTATATE in same patient with multiple bone and soft-tissue metastases.

TABLE 4
Number and Localization of Lesions Detected by Different Imaging Methods

Patient no.	^{111}In-DTPA-octreotide SPECT	^{64}Cu-DOTATATE PET	CT	Follow-up*
1	Peritoneal carcinomatosis, bones (1), lymph nodes (8)	Peritoneal carcinomatosis, bones (>10), lymph nodes (>30) + lungs (6)†	Peritoneal carcinomatosis, bones (1), lymph nodes (>25), lungs (1)†	
2	Negative	Negative	Negative	
3	Large solitary peritoneal soft-tissue mass (1)	Large solitary peritoneal soft-tissue mass (1)	Large solitary peritoneal soft-tissue mass (1)	
4	Negative	Negative	Negative	
5	Lymph nodes (9)	Lymph nodes (>30)	Lymph nodes (10)	
6	Liver (6), large solitary peritoneal soft-tissue mass (1)	Liver (>10), large solitary peritoneal soft-tissue mass (1)	Liver (2)	
7	Pancreas (1), liver (>10), bones (5)	Pancreas (1), liver (>10), bones (>10)	Pancreas (1), liver (>10), bones (1)	
8	Breasts (>10), large solitary peritoneal soft-tissue mass (1), lymph nodes (1)	Breasts (>10), large solitary peritoneal soft-tissue mass (1), lymph nodes (19) + liver (>10)† + bones (1)†	Breasts (>10), large solitary peritoneal soft-tissue mass (1), lymph nodes (12) + liver (2)†	Bones†
9	Liver (1), large solitary peritoneal soft-tissue mass (1)	Liver (1), large solitary peritoneal soft-tissue mass (1) + bones (3)‡ + lymph nodes (2)†	Liver (1)	Lymph nodes†
10	Lymph nodes (8)	Lymph nodes (10)	Lymph nodes (4)	
11	Liver (>10)	Liver (>10)	Liver (10)	
12	Ileum (1), liver (>10), bones (4), lymph nodes (2)	Ileum (1), liver (>10), bones (7), lymph nodes (6) + peritoneal carcinomatosis†	Ileum (1), liver (>10), lymph nodes (4)	Peritoneal carcinomatosis†
13	Lymph nodes (1), thyroid gland (1)	Lymph nodes (1), thyroid gland (1) + pancreas (3)† + lungs (4)†	Lymph nodes (3)+ lungs (10)†	Pancreas†
14	Liver (1), large solitary peritoneal soft-tissue mass (1), peritoneal carcinomatosis	Liver (1), large solitary peritoneal soft-tissue mass (1), peritoneal carcinomatosis + brain (1)† + bones (1)‡	Liver (1), large solitary peritoneal soft-tissue mass (1), peritoneal carcinomatosis	Brain†

*Confirmation by follow-up with CT (coregistered, stand-alone).
†Additional findings detected by PET method.
‡Bone lesions in patients 9 and 14 have not been confirmed yet.
If lesions were known from previous investigations, confirmation was not demanded (Table 1). Besides abdominal SPECT, thoracic SPECT was performed in patients 1, 5, 7, 8, 10, 11, 13, and 14. Numbers are given in parentheses.

comparison of the 2 different nuclear imaging techniques demonstrated a superiority for ^{64}Cu-DOTATATE PET with respect to lesion detection. Promising results from an earlier imaging study using ^{64}Cu-TETA-octreotide(where TETA is 1,4,8,11-tetraazacyclotetradecane-N,N′,N″,N′″-tetraacetic acid in 8 NET patients have previously been reported (*25*). In line with the observations from the present study, SRI using a ^{64}Cu-linked somatostatin analog yielded a higher lesion detection rate than ^{111}In-DTPA-octreotide SPECT. Judged solely on the published images, the image quality obtained with ^{64}Cu-DOTATATE PET seemed to be somewhat better than that obtained with ^{64}Cu-TETA-octreotide. A higher avidity of ^{64}Cu-DOTATATE at somatostatin receptor 2 is therefore likely and would be congruent with the findings of preclinical receptor studies (*13,14*). Moreover, the administered activity of ^{64}Cu-TETA-octreotide was lower than that applied in the current study. The comparison between different PET-based somatostatin analogs can only be speculative given the conflicting results between in vitro receptor affinity studies and in vivo studies in animals and humans. Although it is evident that choice of chelator, isotope, and somatostatin analog affects affinity (*13*), studies in

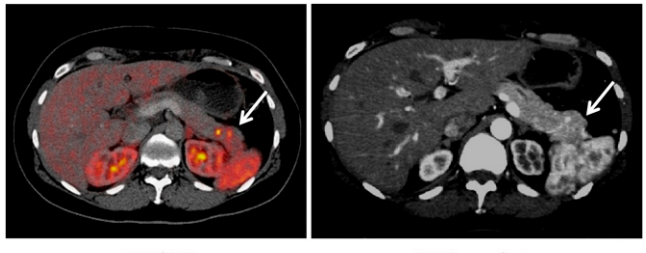

FIGURE 3. Early detection of pancreatic NET on ^{64}Cu-DOTATATE PET/CT. Tumor was not confirmed until 6 mo later on contrast-enhanced CT. Arrow indicates pancreatic NET.

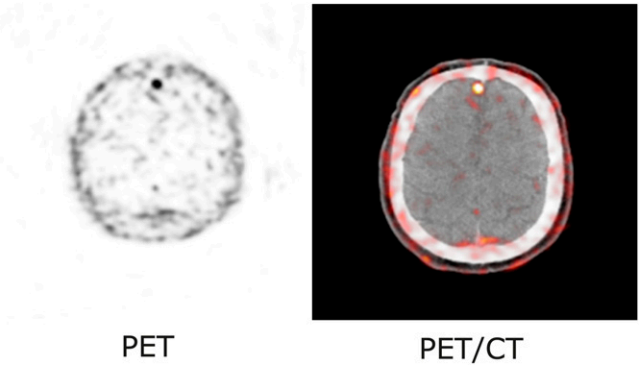

FIGURE 4. Cerebral metastasis demonstrated on ^{64}Cu-DOTATATE PET and PET/CT. Lesion was not seen on SPECT.

patients have not confirmed that higher affinity *per se* translates into better images (*26*). In general, ^{68}Ga-DOTATATE and ^{68}Ga-DOTATOC also perform better than ^{111}In-DTPA-octreotide (*2,10*). Therefore, whether our new tracer is superior to the ^{68}Ga-based tracers can be demonstrated only in a head-to-head comparison. On the basis of such a study, and considering the availability of cyclotron-produced ^{64}Cu versus generator-produced ^{68}Ga, the final choice may then be made.

Several studies have demonstrated somatostatin receptor agonists becoming internalized specifically and early when bound to G-protein receptors (*27,28*). A high and quite stable SUVmax for lesions on both early (1 h) and delayed (3 h) images suggests a high rate of tracer internalization and a low dissociation rate of ^{64}Cu-DOTATATE from somatostatin receptors during this time interval. Moreover, this SUV stability illustrates sufficient in vivo stability of our tracer for imaging purposes. However, increasing hepatic activity is probably caused by dissociation of $^{64}Cu^{2+}$ from the chelator–peptide conjugate. Because the TBR was relatively stable from 1 h on, 1 h images may be used for routine imaging. However, 3 h images offer less activity in the kidneys and urinary tract and still have excellent quality and may also be used for routine purposes. In this clinical setup, ^{64}Cu-DOTATATE PET was capable of visualizing the extent of disease in NET patients more accurately than when evaluated by ^{111}In-DTPA-octreotide SPECT. The clinical significance of this finding remains to be established in larger, prospective studies. The physical half-life of ^{64}Cu (12.7 h) makes ^{64}Cu-DOTATATE a suitable radiopharmaceutical for centralized production and distribution.

CONCLUSION

In this first-in-humans study, we found ^{64}Cu-DOTATATE PET useful for clinical somatostatin receptor imaging. Compared with ^{111}In-DTPA-octreotide SPECT, ^{64}Cu-DOTATATE PET provided superior image quality, detected more (true-positive) lesions, and was associated with a lower radiation burden. Imaging can be performed as early as 1 h after injection, and because of the intermediate half-life of the tracer, it may be produced centrally and distributed, ready to use, to clinical centers.

DISCLOSURE STATEMENT

The costs of publication of this article were defrayed in part by the payment of page charges. Therefore, and solely to indicate this fact, this article is hereby marked "advertisement" in accordance with 18 USC section 1734.

ACKNOWLEDGMENTS

This work was supported by the John and Birthe Meyer Foundation, the Danish National Advanced Technology Foundation, the Research Foundation of Rigshospitalet, the Capital Region of Denmark, the Novo Nordisk Foundation, the Lundbeck Foundation, the A.P. Moeller Foundation, the Svend Andersen Foundation, and the Danish Medical Research Council. No other potential conflict of interest relevant to this article was reported.

REFERENCES

1. Shi W, Johnston CF, Buchanan KD, et al. Localization of neuroendocrine tumours with [^{111}In] DTPA-octreotide scintigraphy (Octreoscan): a comparative study with CT and MR imaging. *QJM.* 1998;91:295–301.
2. Gabriel M, Decristoforo C, Kendler D, et al. ^{68}Ga-DOTA-Tyr3-octreotide PET in neuroendocrine tumors: comparison with somatostatin receptor scintigraphy and CT. *J Nucl Med.* 2007;48:508–518.
3. Binderup T, Knigge U, Loft A, et al. Functional imaging of neuroendocrine tumors: a head-to-head comparison of somatostatin receptor scintigraphy, ^{123}I-MIBG scintigraphy, and ^{18}F-FDG PET. *J Nucl Med.* 2010;51:704–712.
4. Reubi JC, Waser B, Schaer JC, Laissue JA. Somatostatin receptor sst1-sst5 expression in normal and neoplastic human tissues using receptor autoradiography with subtype-selective ligands. *Eur J Nucl Med.* 2001;28:836–846.
5. Krenning EP, Kwekkeboom DJ, Bakker WH, et al. Somatostatin receptor scintigraphy with [^{111}In-DTPA-D-Phe1]- and [^{123}I-Tyr3]-octreotide: the Rotterdam experience with more than 1000 patients. *Eur J Nucl Med.* 1993;20:716–731.
6. Pfeifer AK, Gregersen T, Gronbaek H, et al. Peptide receptor radionuclide therapy with Y-DOTATOC and ^{177}Lu-DOTATOC in advanced neuroendocrine tumors: results from a Danish cohort treated in Switzerland. *Neuroendocrinology.* 2011;93:189–196.
7. Bombardieri E, Ambrosini V, Aktolun C, et al. ^{111}In-pentetreotide scintigraphy: procedure guidelines for tumour imaging. *Eur J Nucl Med Mol Imaging.* 2010;37:1441–1448.
8. Balon HR, Brown TL, Goldsmith SJ, et al. The SNM practice guideline for somatostatin receptor scintigraphy 2.0. *J Nucl Med Technol.* 2011;39:317–324.
9. Virgolini I, Ambrosini V, Bomanji JB, et al. Procedure guidelines for PET/CT tumour imaging with ^{68}Ga-DOTA-conjugated peptides: ^{68}Ga-DOTA-TOC, ^{68}Ga-DOTA-NOC, ^{68}Ga-DOTA-TATE. *Eur J Nucl Med Mol Imaging.* 2010;37:2004–2010.
10. Srirajaskanthan R, Kayani I, Quigley AM, Soh J, Caplin ME, Bomanji J. The role of ^{68}Ga-DOTATATE PET in patients with neuroendocrine tumors and negative or equivocal findings on ^{111}In-DTPA-octreotide scintigraphy. *J Nucl Med.* 2010;51:875–882.
11. Schäfers KP. The promise of nuclear medicine technology: status and future perspective of high-resolution whole-body PET. *Phys Med.* 2008;24:57–62.
12. Townsend DW. Physical principles and technology of clinical PET imaging. *Ann Acad Med Singapore.* 2004;33:133–145.
13. Reubi JC, Schar JC, Waser B, et al. Affinity profiles for human somatostatin receptor subtypes SST1-SST5 of somatostatin radiotracers selected for scintigraphic and radiotherapeutic use. *Eur J Nucl Med.* 2000;27:273–282.
14. Li WP, Lewis JS, Kim J, et al. DOTA-D-Tyr(1)-octreotate: a somatostatin analogue for labeling with metal and halogen radionuclides for cancer imaging and therapy. *Bioconjug Chem.* 2002;13:721–728.

15. Binderup T, Knigge U, Mellon Mogensen A, Palnaes Hansen C, Kjaer A. Quantitative gene expression of somatostatin receptors and noradrenaline transporter underlying scintigraphic results in patients with neuroendocrine tumors. *Neuroendocrinology.* 2008;87:223–232.
16. Thisgaard H, Jensen M, Elema DR. Medium to large scale radioisotope production for targeted radiotherapy using a small PET cyclotron. *Appl Radiat Isot.* 2011;69:1–7.
17. Sobin LH, Gospodarowicz MK, Wittekind C. *UICC: TNM Classification of Malignant Tumours, Seventh ed.*Oxford, U.K.:Wiley-Blackwell; 2009: 94–99.
18. Rindi G, Kloppel G, Alhman H, et al. TNM staging of foregut (neuro)endocrine tumors: a consensus proposal including a grading system. *Virchows Arch.* 2006;449:395–401.
19. Rindi G, Kloppel G, Couvelard A, et al. TNM staging of midgut and hindgut (neuro) endocrine tumors: a consensus proposal including a grading system. *Virchows Arch.* 2007;451:757–762.
20. Stabin MG, Sparks RB, Crowe E. OLINDA/EXM: the second-generation personal computer software for internal dose assessment in nuclear medicine. *J Nucl Med.* 2005;46:1023–1027.
21. International Commission on Radiological Protection. ICRP publication 60: recommendations of the International Commission on Radiological Protection. *Ann ICRP.* 1991;21:1–3.
22. Disselhorst JA, Brom M, Laverman P, et al. Image-quality assessment for several positron emitters using the NEMA NU 4-2008 standards in the Siemens Inveon small-animal PET scanner. *J Nucl Med.* 2010;51:610–617.
23. Sánchez-Crespo A, Andreo P, Larsson SA. Positron flight in human tissues and its influence on PET image spatial resolution. *Eur J Nucl Med Mol Imaging.* 2004;31:44–51.
24. Soret M, Bacharach SL, Buvat I. Partial-volume effect in PET tumor imaging. *J Nucl Med.* 2007;48:932–945.
25. Anderson CJ, Dehdashti F, Cutler PD, et al. ^{64}Cu-TETA-octreotide as a PET imaging agent for patients with neuroendocrine tumors. *J Nucl Med.* 2001;42:213–221.
26. Poeppel TD, Binse I, Petersenn S, et al. ^{68}Ga-DOTATOC versus ^{68}Ga-DOTATATE PET/CT in functional imaging of neuroendocrine tumors. *J Nucl Med.* 2011;52:1864–1870.
27. Ginj M, Zhang H, Eisenwiener KP, et al. New pansomatostatin ligands and their chelated versions: affinity profile, agonist activity, internalization, and tumor targeting. *Clin Cancer Res.* 2008;14:2019–2027.
28. Waser B, Tamma ML, Cescato R, Maecke HR, Reubi JC. Highly efficient in vivo agonist-induced internalization of sst2 receptors in somatostatin target tissues. *J Nucl Med.* 2009;50:936–941.

The Journal of NUCLEAR MEDICINE

Clinical PET of Neuroendocrine Tumors Using ^{64}Cu-DOTATATE: First-in-Humans Study

Andreas Pfeifer, Ulrich Knigge, Jann Mortensen, Peter Oturai, Anne Kiil Berthelsen, Annika Loft, Tina Binderup, Palle Rasmussen, Dennis Elema, Thomas Levin Klausen, Søren Holm, Eric von Benzon, Liselotte Højgaard and Andreas Kjaer

J Nucl Med. 2012;53:1207-1215.
Published online: July 10, 2012.
Doi: 10.2967/jnumed.111.101469

The Journal of Nuclear Medicine is published monthly.
SNMMI | Society of Nuclear Medicine and Molecular Imaging
1850 Samuel Morse Drive, Reston, VA 20190.
(Print ISSN: 0161-5505, Online ISSN: 2159-662X)

SNMMI SOCIETY OF NUCLEAR MEDICINE AND MOLECULAR IMAGING